MICROSTRIP ANTENNA'S GAIN ENHANCEMENT USING LEFT-HANDED METAMATERIAL STRUCTURE

H. A. Majid, M. K. A. Rahim, and T. Masri

Faculty of Electrical Engineering
Universiti Teknologi Malaysia
Skudai, Johor 81310, Malaysia

Abstract—The design, simulation and fabrication of a left-handed metamaterial (LHM) structure is presented. The combination of the modified square rectangular Split Ring Resonator (SRR) and the Capacitance Loaded Strip (CLS) were used to obtain the negative value of permeability, μ and the negative permittivity, ε. Nicolson-Ross-Wier approach was used to identify the double negative region. A good agreement between simulated and measured results has been achieved. Upon incorporation with a single patch microstrip antenna, the performance of the antenna was improved where the gain of the microstrip antenna was increased up to 4 dB, and its bandwidth widens from 2.9% to 4.98%. These improvements are due to the negative refraction characteristics of the LHM structure that acts as a lens when placed in front of the antenna.

1. INTRODUCTION

Left-handed metamaterial (LHM) is a material whose permeability and permittivity are simultaneously negative. LHM is an interesting material to be investigated where this artificial material has several unique properties especially the backward wave and negative refraction. The backward wave propagation has been verified by [1], and the negative refraction has been proven by [2, 3]. The history of LHM starts by Veselago [4] when he made a theoretical speculation of this artificial material that exhibits negative permittivity and permeability. Thirty four years later, in 2001, Smith made the first prototype structures of LHM [5]. The LHM is a combination of (SRR) and thin wires (TW). New structures have been proposed such as

---

Corresponding author: H. A. Majid (huda_set@yahoo.com).

Omega shape, spiral multi-split, fishnet and S-shape, and they exhibit the properties of a LHM [6–8]. Since then, many researchers have been interested in investigating this artificial material, and several of them used the LHM to improve the properties of the microwave devices such as antennas and filters [9]. Many papers have been published regarding the LHM integrated with antennas, and their properties have been analyzed [10–12]. Although other metamaterials such as FSS and EBG have been used to enhance the gain of an antenna [13, 14], the focusing effect of a LHM can be exploited in order to improve the directivity and gain of an antenna [15–17].

In this work, a study has been made to discuss and analyze the properties of the LHM structure and the performance of a single patch microstrip antenna with and without the LHM structure. The LHM structure's design consists of a combination of modified SRR and CLS, as illustrated in the diagram in Figure 1. The CLS has an extra capacitance and produces a lower stop-band [18]. Both the LHM and antenna have been designed to operate at 2.4 GHz.
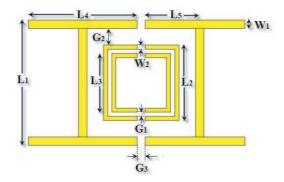
Figure 1. Dimension of LHM structure consists of SRR and CLS.

Figure 1 illustrates the LHM structure which consists of a combination of a modified SRR and two CLS.

The widths and gaps of the SRR transmission lines, W_2 and G_1, are fixed to 0.5 mm. The gap between the two CLSs, G_3, is 1 mm, and the width of CLS transmission lines, W_1, is 1 mm. The gap between the SRR and CLS, G_2, is 2 mm. The height of the CLS inclusions, L_1, is 15.1 mm. The length of the full capacitance strips, L_4, is 13.1 mm, and the length of the half strips, L_5, is 6.55 mm. The length of the outer SRR, L_2, is 9.1 mm, and the inner length of the SRR, L_3, is 7.1 mm. The dielectric constant of the FR4 substrate is 4.7, with a thickness of 1.6 mm and tangential loss of 0.019.

The modified SRR produces magnetic material-like responses and

exhibits a negative permittivity. This magnetic moment exhibits a plasmonic-type of frequency in the form of [10, 19]:

$$\mu\left(\omega\right) = \mu_0\left(1 - \frac{\omega_{pm}^2}{\omega\left(\omega - j\Gamma_m\right)}\right) \tag{1}$$

where;
$\omega_{pm} =$ Magnetic plasma frequency,
$\Gamma_m =$ Damping coefficient,
$\mu_0 =$ Permeability in free-space.
    The SRR would yield a negative value of permeability when $\omega < \omega_{pm}$.
    On the other hand, the CLS produces strong dielectric-like responses and exhibits a negative permeability [5]. This circumstances generate an electric dipole moment to the structure and exhibit a plasmonic-type of permittivity frequency in a function of [19]:

$$\varepsilon\left(\omega\right) = \varepsilon_0\left(1 - \frac{\omega_{pe}^2}{\omega\left(\omega - j\Gamma_e\right)}\right) \tag{2}$$

where;
$\omega_{pe} =$ Electric plasma frequency,
$\Gamma_e =$ Damping coefficient,
$\varepsilon_0 =$ Permittivity at free-space.
    The CLS would yield a negative value of permittivity when $\omega < \omega_{pe}$.

2. SIMULATION RESULTS

2.1. Simulation of the LHM Unit Cell

The simulation of the LHM is executed using Computer Simulation Technology (CST) software. Figure 2 illustrates the simulation setup for the unit cell of the LHM. Perfect magnetic conductor (PMC) boundary condition is set on the left and right faces of the box, and perfect electric conductor (PEC) boundary condition is set on the top and bottom of the box. The incident wave propagates in z-axis direction, while the E-field of the incident wave is polarized along y-axis, and the H-field of the incident wave is polarized along x-axis. The gaps between each slab are set to 16 mm.
    The S-parameters that were obtained from the simulation were exported to MathCAD software. Nicholson, Ross and Weir (NRW) approach are used to determine the permittivity and permeability of
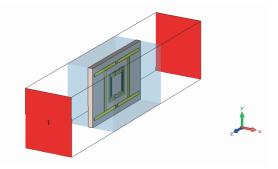
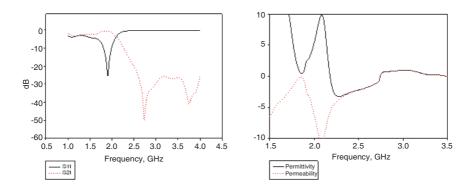**Figure 2.** The LHM simulation setup.

Figure 3. Value of S_{11} and S_{21}.

Figure 4. Value of ε_r and μ_r of the single cell LHM.

the LHM structure, and the results obtained are as shown in Figure 3 and Figure 4. Initially, the basic equations used to determine the ε_r and μ_r are shown below [20]:

$$\varepsilon_r \approx \frac{2}{jk_0 d}\frac{1 - \nu_1}{1 + \nu_1} \tag{3}$$

$$\mu_r \approx \frac{2}{jk_0 d}\frac{1 - \nu_2}{1 + \nu_2} \tag{4}$$

where:
$v_1 = S_{21} + S_{11}$,
$v_2 = S_{21} - S_{11}$,
$k_0 = \omega/c$,
$w = \text{Radian frequency,}$

$d =$ Slab thickness,
$c =$ Speed of light.

Figure 3 shows the simulated results of S_{11} and S_{21}. Referring to Figure 4, the range of the negative permittivity and permeability (-ε and -μ) starts from 2.18 GHz to 2.74 GHz. To investigate the focusing effect of the LHM structures, a single patch microstrip antenna has been designed, where the operating frequency is within the range of negative permittivity and permeability. The centre frequency of 2.4 GHz is chosen as the operating frequency of the microstrip antenna.

2.2. Single Patch Microstrip Antenna Incorporated with the LHM

Figure 5 shows the LHM incorporated with the microstrip antenna. The overall dimensions of the antenna incorporated with the LHM structure as shown in Figure 6 are 117 mm × 127 mm × 41.6 mm. The LHM structures are placed in front of the microstrip antenna with a gap distance of 12.5 mm from the ground plane. The simulated return loss S_{11} of the antenna with and without the LHM structure is as shown in Figure 7. The return loss seems to shift to a higher region when the antenna is incorporated with the LHM, but it still shows a good agreement between microstrip antenna with and without LHM, where in both conditions, the antenna still operates at 2.4 GHz. The bandwidth of the antenna increases after the incorporation with LHM from 2.5% to 4%.
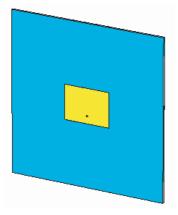

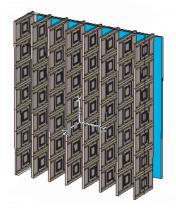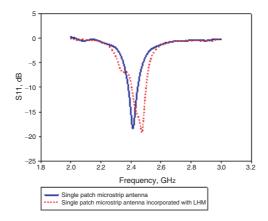**Figure 5.** Single patch antenna operated at 2.4 GHz.

Figure 6. Single patch antenna integrated with LHM structure.

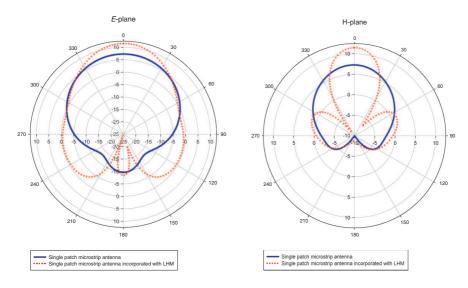**Figure 7.** Return loss S_{11} of the single patch microstrip antenna with and without LHM.

Figure 8. Simulated radiation pattern in E-plane.

Figure 9. Simulated radiation pattern in H-plane.

Figure 8 shows the radiation pattern of microstrip antenna with and without LHM in E-plane, while Figure 9 shows the radiation pattern of microstrip antenna with and without LHM in H-plane. An increasing gain up to 4.11 dB is visible only by attaching the LHM in front of the microstrip antenna. The 3 dB beamwidth in E-plane becomes narrower from $78°$ to $48.5°$ and also in H-plane, from $78.7°$ to $34.3°$. The side lobes are also visible.

2.3. *E*-field Analysis in the Present of LHM in Front of the Single Patch Microstrip Antenna

Figure 10(a) shows the *E*-field of a typical microstrip antenna operating at 2.4 GHz in *E*-plane, while Figure 10(b) shows the *E*-field of the antenna incorporated with LHM in the *E*-plane. Figure 11(a) shows the *E*-field of the microstrip antenna, while Figure 11(b) shows the *x*-plane *E*-field of the antenna incorporated with LHM. It was observed that the *E*-field is more directed once it left the LHM. The LHM had the ability to focus the waves, and this in turn explained the gain increase in the antenna.
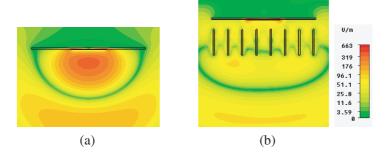

(a)   (b)

Figure 10. (a) Observation on *E*-field in *E*-plane for the single patch microstrip antenna and (b) observation on *E*-field in *E*-plane for the single patch microstrip antenna incorporated with LHM.

(a)   (b)

Figure 11. (a) Observation on *E*-field in *H*-plane for the single patch microstrip antenna and (b) observation on *E*-field in *H*-plane for the single patch microstrip antenna incorporated with LHM.
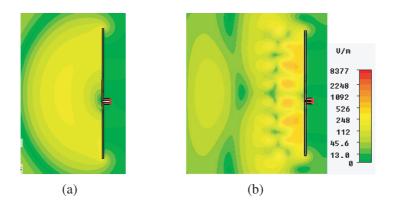
3. FABRICATION AND MEASURED RESULTS

Figure 12 shows the fabricated microstrip antenna, and Figure 13 shows the fabricated antenna incorporated with the LHM structure. The fabrication is done using wet etching technique, and both the microstrip antenna and LHM structure are measured at an operating frequency of 2.4 GHz.
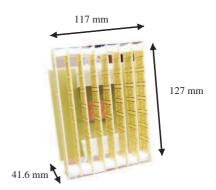

Figure 12. Single patch microstrip antenna.

117 mm

127 mm

41.6 mm

Figure 13. Single patch microstrip antenna integrated with LHM structure.

The return loss, S_{11}, for single patch microstrip antenna with and without LHM at 2.4 GHz is shown in Figure 4. The measured bandwidth of single patch microstrip antenna, incorporated with the LHM, is much wider than the single patch microstrip antenna, as predicted in the simulation. Figure 15 shows the measured gain (S_{21}) for both antennas. An increment up to 4.366 dB at 2.4 GHz is noticed from the graph. The gain comparison is measured using network analyzer in an anechoic chamber.

Figure 16 shows the comparison of the radiation patterns for both antennas in E-plane, and Figure 17 shows the comparison of radiation pattern in H-plane. From observation, the gain of the antenna increased up to 4 dB after the incorporation of the LHM. The 3 dB beamwidth for E-plane becomes narrower from $90°$ to $56°$, and in H-plane, the 3 dB beamwidth narrows up to $38°$ from $83°$. The measured results show a good agreement with the simulated ones where the gain increases up to 4 dB while the 3 dB beamwidth becomes narrower.
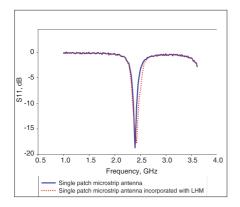
Figure 14. Return loss S_{11} of the single patch microstrip antenna with and without LHM.
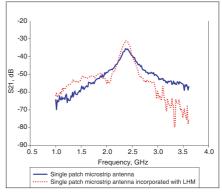

Figure 15. Gain (S_{21}) comparison between the single patch microstrip antenna with and without LHM.
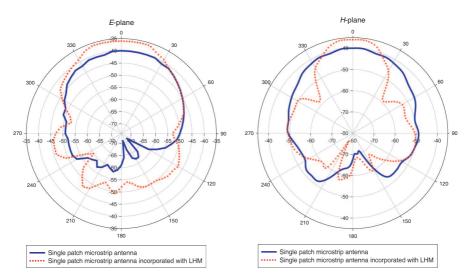

Figure 16. Measured radiation pattern in E-plane.

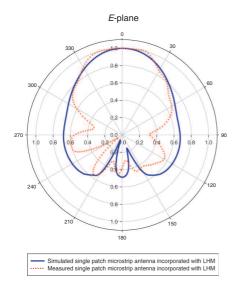**Figure 17.** Measured radiation pattern in H-plane.

4. COMPARISON BETWEEN SIMULATED AND MEASURED RESULTS

Table 1 shows the comparison between the simulated and measured results of the same type of antenna, incorporated with the LHM

structures. The results of simulation and measurement in term of gain increment are similar. The other results are all different between the simulated and measured results due to the tolerances of the dielectric constant of the materials used and imperfection during fabrication process.

Figures 18 and 19 show the radiation pattern in E- and H-planes for both simulated and measured antennas incorporated with LHM. The shape of the simulated radiation pattern is approximately similar to the measured radiation pattern.

Table 1. Comparison between simulated and measured single patch microstrip antenna incorporated with LHM.

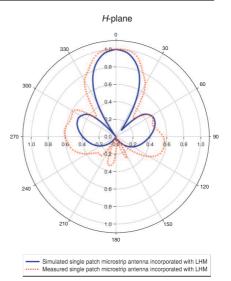| Antenna parameters at 2.4 GHz		Simulated single patch microstrip antenna incorporated with LHM	Measured single patch microstrip antenna incorporated with LHM
Return loss, S_{11}		-10 dB	-15.71 dB
Bandwidth		4%	4.98%
Gain increment		4.22 dB	4 dB
3 dB beam-width	E-plane	48.5°	56°
	H-plane	34.3°	38°
Front to back lobe ratio		19.94 dB	17 dB

Figure 18. Comparison between simulated and measured radiation patterns in E-plane.

Figure 19. Comparison between simulated and measured radiation patterns in H-plane.

5. CONCLUSION

As a conclusion, the performance of the antenna has been improved through the incorporation with the LHM structures. The radiation pattern of microstrip antenna integrated with LHM structure has an improved gain compared to the gain of the microstrip antenna without LHM structure. An improvement of 4 dB gain in simulation and measurement is obtained when LHM is placed in front of the microstrip antenna. The measured bandwidth of the antenna is widened from 2.9% to 4.98%. The 3 dB half-power beamwidth (HPBW) of the single patch microstrip antenna with LHM structure is narrower than that of the antenna without the LHM structures, where the single patch microstrip antenna has a HPBW of 80°, and with LHM structures, it narrowed down to 40°. This shows that LHM acts as a focusing device where the beam became narrower, and the gain increased. However, despite the increment of the gain, a bigger side and back lobe was also observed. If the side and back lobe can be reduced, the gain of the microstrip antenna with LHM structure could be further improved.

ACKNOWLEDGMENT

REFERENCES

1. Carbonell, J., L. J. Rogla, V. E. Boria, and D. Lippens, "Design and experimental verification of backward-wave propagation in periodic waveguide structures," *IEEE Transactions on Microwave Theory and Techniques*, Vol. 54, No. 4, 1527–1533, April 2006.

2. Aydin, A., G. Kaan, and O. Ekmel, "Two-dimensional left-handed metamaterial with a negative refractive index," *Journal of Physics Conference Series*, Vol. 36, 6–11, 2006.

3. Shelby, R. A., D. R. Smith, and S. Shultz, "Experimental verification of a negative index of refraction," *Science*, Vol. 292, 77–79, 2001.

4. Veselago, V. G., "The electrodynamics of substances with simultaniously negative values of permittivity and permeability," *Sov. Phys. Usp.*, Vol. 10, 509, 1968.

5. Smith, D. R., W. J. Padilla, D. C. Vier, S. C. Nemat-Nasser,

and S. Schultz, "Loop-wire medium for investigating plasmons at microwave frequency," *Phys. Rev. Lett.*, Vol. 84, 4184, 2000.

6. Wu, B.-I., W. Wang, J. Pacheco, X. Chen, T. Grzegorczyk, and J. A. Kong, "A study of using metamaterials as antenna substrate to enhance gain," *Progress In Electromagnetics Research*, PIER 51, 295–328, 2005.

7. Alici, K. B., F. Bilotti, L. Vegni, and E. Ozbay, "Optimazation and tunability of deep subwavelength resonators for metamaterial application: Complete enhanced transmission through a subwavelength aperture," *Opt. Express*, Vol. 17, 5933–5943, 2009.

8. Alici, K. B. and E. Ozbay, "Chareacterization and tilted response of a fishnet metamaterial operating at 100 GHz," *J. Phys. D: Appl. Phys.*, Vol. 41, 135011, 2008.

9. Gil, M., J. Bonache, J. Selga, J. Garcia-Garcia, and F. Martin, "High-pass filters implemented by composite right/left handed (CRLH) transmission lines based on complementary split rings resonators (CSRRs)," *PIERS Online*, Vol. 3, No. 3, 251–253, 2007.

10. Buell, K., H. Mosallaei, and K. Sarabandi, "A substrate for small patch antennas providing tunable miniaturization factor," *IEEE Trans. Microwave Theory Tech.*, Vol. 54, 135, 2006.

11. Alici, K. B. and E. Ozbay, "Electrically small split ring resonator antennas," *J. Appl. Phys.*, Vol. 101, 083104, 2007.

12. Alu, A., F. Bilotti, N. Engheta, and L. Vegni, "Subwavelength, compact, resonant patch antennas loaded with metamaterials," *IEEE Transactions on Antennas and Propagation*, Vol. 55, 13, 2007.

13. Pirhadi, A., F. Keshmiri, M. Hakkak, and M. Tayarani, "Analysis and design of dual band high directivity EBG resonator antenna using square loop FSS as superstrate layer," *Progress In Electromagnetics Research*, PIER 70, 1–20, 2007.

14. Yoo, K., R. Mitra, and N. Farahat, "A novel technique for enhancing the directivity of microstrip patch antennas using an EBG superstrate," *IEEE Antennas & Propagation Society International Symposium*, 1–4, 2008.

15. Erentok, A., P. L. Luljak, and R. W. Ziolkowski, "Characterization of a volumetric metamaterial realization of an artificial magnetic conductor for antenna application," *IEEE Transactions on Antennas and Wireless Propagation*, Vol. 53, No. 1, 160–172, 2005.

16. Burokur, S. N., M. Latrach, and S. Toutain, "Theorical investigation of a circular patch antenna in the presence of a left-

handed mematerial," *IEEE Antennas and Wireless Propagation Letters*, Vol. 4, 183–186, 2005.

17. Li, B., B. Wu, and C.-H. Liang, "Study on high gain circular waveguide array antenna with metamaterial structure," *Progress In Electromagnetics Research*, PIER 60, 207–219, 2006.

18. Wongkasem, N. and A. Akyurtlu, "Group theory based design of isotropic negative refractive index metamaterials," *Progress In Electromagnetics Research*, PIER 63, 295–310, 2006.

19. Caloz, C. and T. Itoh, *Electromagnetic Metamaterials Transmission Line Theory and Microwave Applications*, Wiley Inter-Science, 2005.

20. Ziolkowski, R. W., "Design, fabrication, and testing of double negative metamaterials," *IEEE Transactions on Antennas and Wireless Propagation*, Vol. 51, No. 7, 1516–1529, 2003.